arXiv:physics/0606169v1 [physics.chem-ph] 20 Jun 2006

Cooperating or Fighting with Control Noise in the Optimal Manipulation of Quantum Dynamics

Feng Shuang and Herschel Rabitz
Department of Chemistry, Princeton University, Princeton, New Jersey 08544

(Dated: February 2, 2008)

Abstract

This paper investigates the impact of control field noise on the optimal manipulation of quantum dynamics. Simulations are performed on several multilevel quantum systems with the goal of population transfer in the presence of significant control noise. The noise enters as run-to-run variations in the control amplitude and phase with the observation being an ensemble average over many runs as is commonly done in the laboratory. A genetic algorithm with an improved elitism operator is used to find the optimal field that either fights against or cooperates with control field noise. When seeking a high control yield it is possible to find fields that successfully fight with the noise while attaining good quality stable results. When seeking modest control yields, fields can be found which are optimally shaped to cooperate with the noise and thereby drive the dynamics more efficiently. In general, noise reduces the coherence of the dynamics, but the results indicate that population transfer objectives can be met by appropriately either fighting or cooperating with noise, even when it is intense.

I. INTRODUCTION

Control of quantum processes is actively being pursued theoretically [1, 2] and experimentally[3, 4]. In practice control field noise and environmental interactions inevitably will be present, and the general expectation is that their involvement will be deleterious towards achieving control[5]. The present paper only considers the influence of field noise upon the controlled dynamics with the noise described by shot-to-shot pulse variations, as in the signal average experiments. A separate work will explore analogous issue for environmental interactions. Recent studies have considered several aspects of the influence of laser noise[6, 7, 8, 9, 10, 11], and this work aims to further explore the issue. Operating under closed loop[12] in the laboratory will naturally deal with the noise as best as possible. Using simple models and simulations, this paper will explore the nature of robustness to noise and the possibility of cooperating with the noise rather than fighting against it, especially in the strong noise limit. Such a prospect has foundation in analogous classical stochastic resonance phenomena[13].

The presence of field noise in quantum control is generally viewed as problematic, but recent successful experiments at least support the point that some noise can be tolerated[14, 15, 16, 17, 18, 19] and that it may have a constructive effect in quantum dynamics[20, 21, 22, 23]. A recent theoretical analysis[7] on the impact of field noise upon optimal control indicated that an inherent degree of robustness can be anticipated by virtue of controlled observable expectation values being bilinear in the evolution operator and its adjoint. Some simulations of closed loop experiments also show that robust control is possible, and that properly designed control fields can fight against noise[6, 24, 25]. In some special circumstances, field noise even may be helpful[26, 27, 28, 29, 30, 31]. The presence of field noise may also improve the convergence rate of the laboratory learning control processes[24, 25].

In this paper, we will investigate four model illustrations of optimal control in the presence of field noise, especially for cases of strong noise. It is naturally found that field noise is deleterious to achieving control if a high yield is desired, however we also find robust high yield solutions that are extremely stable with respect to noise. If a low yield is acceptable, then it is shown that field noise may even be helpful and the control field can cooperate with it. The present work primarily aims to demonstrate these findings in several model illustrations. A follow on paper will analyze the mathematical and physical origin of the observed behavior[32].

Section II will present the model and control formulation used in these studies. Section III describes the genetic algorithm employed to search for an optimal control field in the presence of noise, and some special algorithmic modifications are made for this purpose. Section IV presents a set of control simulations under various system and noise conditions. Some brief concluding remarks are given in section V.

II. THE MODEL SYSTEM

The effect of field noise on controlled quantum dynamics will be explored in the context of population transfer in multilevel systems characterized by the Hamiltonian H,

$$H = H_0 - uE(t) \tag{1a}$$

$$H_0 = \sum_{\upsilon} \varepsilon_{\upsilon} \left|\upsilon\right\rangle \left\langle\upsilon\right| \tag{1b}$$

where $|\upsilon\rangle$ is an eigenstate of H_0 and ε_{υ} is the associated field-free eigen-energy. The noise-free control field $E(t)$ is taken to have the form

$$E_0(t) = S(t) \sum_{l} A_l^0 \cos\left(\omega_l t + \theta_l^0\right), \tag{2a}$$

$$S(t) = \exp\left[-\left(t - T/2\right)^2 / 2\sigma^2\right], \tag{2b}$$

where $\{\omega_l\}$ are the allowed resonant transition frequencies of the system. The controls are the amplitudes $\{A_l^0\}$ and phases $\{\theta_l^0\}$.

In each simulation, a reference noise-free optimal control calculation is first performed with the cost function:

$$J_0\left[E_0(t)\right] = \left|O\left[E_0(t)\right] - O_T\right|^2 + \alpha F_0 \tag{3a}$$

$$F_0 = \sum_{l} \left(A_l^0\right)^2, \tag{3b}$$

where O_T is the target value (expressed as a percent yield in the applications later) and $O\left[E_0(t)\right]$ is the outcome produced by the field $E_0(t)$, and F_0 is the fluence of the control field whose contribution is weighted by the constant, $\alpha > 0$. In the present work, $O = |\Psi_f\rangle \langle\Psi_f|$ is a projection operator for the population of the target state $|\Psi_f\rangle$.

Noise in the laboratory could take on various forms and arise from a number of sources[9]. In keeping with laboratory practice, the achieved control will be measured as an ensemble average over the outcome of many control fields. Here the noise is modeled as run-to-run uncertainties in the amplitudes and phases in Eq.(2a)[6]. This work will take an extreme conservative view to explore the nature of achievable control when such noise is large and independent of each other in the different runs. The noise is simulated by introducing the parameters γ_{A_l} and γ_{θ_l} which are chosen randomly over the range $[-\Gamma_A, \Gamma_A]$ and $[-\Gamma_\theta, \Gamma_\theta]$, respectively,

$$A_l^{(i)} = A_l^0 + \gamma_{A_l}^{(i)}, \quad \theta_l^{(i)} = \theta_l^0 + \gamma_{\theta_l}^{(i)}. \tag{4}$$

What is referred to as "amplitude noise" alone actually allows for phase changes over the range $[-\Gamma_A, \Gamma_A]$. By exploring the case of $\Gamma_\theta \neq 0$, $\Gamma_A = 0$, the phase contribution will become clear. Different random values are selected for the amplitudes and phases over their respective ranges in replicate simulations $i = 1, 2, \cdots, M$ corresponding to an ensemble of M control experiments. The i-th experiment is driven by field

$$E^{(i)}(t) = S(t) \sum_l A_l^{(i)} \cos\left(\omega_l t + \theta_l^{(i)}\right). \tag{5}$$

and the net outcome of all the control experiments is the average,

$$\left\langle O\left[E^{(i)}(t)\right]\right\rangle_N = \frac{1}{M}\sum_{i=1}^{M} \left|\left\langle \psi\left(\left[E^{(i)}(t)\right], T\right) | \psi_f \right\rangle\right|^2, \tag{6}$$

where $\left|\psi\left(\left[E^{(i)}(t)\right], T\right)\right\rangle$ is the final state driven with the i-th field in Eq.(5). The bracket notation $\left[E^{(i)}(t)\right]$ indicates a functional dependence on the field over the internal $0 \leq t \leq T$. The objective function in the presence of noise is:

$$J_N\left(A_l^0, \theta_l^0\right) = \left|\left\langle O\left[E^{(i)}(t)\right]\right\rangle_N - O_T\right|^2 + \alpha F_0. \tag{7}$$

In order to find a robust control field, for which the outcome is optimally insensitive to the noise, we incorporate the measurement standard deviation σ into the cost function to finally produce:

$$J\left(A_l^0, \theta_l^0\right) = J_N\left(1 + \beta\sigma_N\left[E^{(i)}(t)\right]\right), \tag{8}$$

where

$$\sigma_N\left[E^{(i)}(t)\right]=\sqrt{\left\langle O^2\left[E^{(i)}(t)\right]\right\rangle_N-\left\langle O\left[E^{(i)}(t)\right]\right\rangle_N^2} \tag{9}$$

and $\langle O^2\rangle_N$ is defined similar to Eq.(6). The coefficient $\beta > 0$ balances the magnitudes of the terms. Since J is minimized, pulses that produce a small variance in the objective are favored.

III. A GENETIC ALGORITHM WITH AN IMPROVED ELITISM OPERATOR IN THE PRESENCE OF CONTROL NOISE

Current quantum control experiments[12] employ genetic (GA)[33] or evolutionary algorithms[14] to identify optimal control fields. Simulations have shown [24, 25] that GAs can tolerate a high level of noise because they don't make sharp decisions, allowing for decision errors to be averaged out over the generations of the learning process. GAs can be very effective, but they also can be expensive to employ, especially when optimizing a shot-to-shot stochastic process because a large number of experiments are needed to perform the ensemble average. Many of the simulations in this work include significant field noise, and it was found that at least $M = 10^4$ runs are needed to get accurate ensemble averages. In order to speed up the simulations, many strategies have been proposed[34, 35, 36]. Here we used a simple approach: only perform full statistical averaging with the most effective field at each generation, while for intermediate assessments of all other individuals use a small number of ensemble average runs. The detailed procedure to select an optimal field consists of the following steps:

1. Initialize the GA. We assume there are two special individuals, one is denoted as "*best*", which is the best member of population; another is denoted as "*elitist*", which will be updated in each generation. *elitist* is the same as *best* when the GA starts.

2. Perform the standard operations of reproduction, crossover and mutation to generate a new population for the next generation. Evaluate the fitness of each individual in the population with a small size ensemble ($M \leq 10^3$ in this work).

3. Compare the objective values arising from *elitist* and *best* (the best member of the new generation):

if J(*elitist*) $\leq$ J(*best*) then re-evaluate the cost function of *elitist* with a large ensemble ($M \geq 10^4$ in this work);

if $J(elitist) > J(best)$ then re-evaluate the cost function of *best* with a large ensemble ($M \geq 10^4$ in this work);

4. Compare the updated cost function value of *elitist* and *best* from the last step;

if $J(elitist) \leq J(best)$ then replace the worst member of population with *elitist*

if $J(elitist) > J(best)$ then set $elitist = best$;

5. Go to step 2, and repeat the GA operations until convergence is fulfilled.

Although there is always a chance that a good field is overlooked by this procedure, it proved to be effective in finding robust fields. The procedure is very efficient as it only performs extensive statistical averaging on the likely most effective fields.

IV. NUMERICAL SIMULATIONS

To demonstrate how quantum optimal control can either fight or cooperate with field noise, we performed four simulations with simple model systems. The first three simulations use the single path system in Figure 1(a) while the last simulation uses the double-path system in Figure 1(b). Equation (8) is the cost function used to the guide GA choice of the control field. The average yields shown in all the tables typically involve an ensemble of $M = 10^4$ samples. The simulations used the Toolkit technique[37] to efficiently solve the Schrödinger equation.

A. Model 1

This model used the single path 5-level system in Figure 1(a) with eigenstates $|i\rangle$, $i = 0, \cdots, 4$ of the field free Hamiltonian H_0, having only nearest neighbor transitions with the frequencies $\omega_{01} = 1.511$, $\omega_{12} = 1.181$, $\omega_{23} = 0.761$, $\omega_{34} = 0.553$ in rad·fs^{-1}, and associated transition dipole moments $\mu_{01} = 0.5855$, $\mu_{12} = 0.7079$, $\mu_{23} = 0.8352$, $\mu_{34} = 0.9281$ in 1.0×10^{-30} C·m. The target time is $T = 200$ fs, and the pulse width in Eq.(5) is $s = 30$ fs. The control objective is to transfer the population from the initially prepared ground state $|0\rangle$ to the final state $|4\rangle$, such that $O = |4\rangle\langle 4|$. As a reference control case, the algorithm is run first without any field noise using the cost function in Eq.(3a). Figure 2 shows the optimal field for the two separate goals $O_T = 100\%$ and 2.25%. These two extreme cases of high and low target yield are chosen to illustrate their distinct control behavior in the present of noise. The choice of the low yield target of 2.25% is arbitrary with similar behavior found for yields up to $\sim$ 10%. In some applications even making a modest yield of a particular product or state for study would be significant. The physical criteria in the low yield limit is that sufficient noise be present to produce at least a small population in the target state. At the target time, the noise free fields in Figures 2(a1) and 2(b1) drive 98.7% and 2.2% of the population to target state, respectively.

In order to calibrate the strength of the noise, Table I shows the state population distributions when the system is only driven by noise of various amplitudes. When $\Gamma_A > 0.07$, the influence of the field noise is very large as it drives more than 40% population out of the ground state. To examine the influence of noise when seeking an optimal control field, first consider the case of aiming for a high yield (i.e., perfect control with the target yield set at $O_T = 100\%$ in Eq.(7)). Table II shows how the optimal control fields fight with different types of noise in this case. In order to reveal the separate contributions of noise upon the optimally controlled dynamics, Table II shows the yield from noise alone $\left\langle O\left[E_n^{(i)}(t)\right]\right\rangle_N$ without the control field being present. Here $E_n^{(i)}(t)$ is the i-th member of a pure field noise ensemble:

$$E_n^{(i)}(t) = S(t)\sum_l \gamma_{A_l}^{(i)} \cos\left(\omega_l t + \gamma_{\theta_l}^{(i)}\right). \tag{10}$$

The control field is determined optimally in the presence of noise; as a reference, the yield $O\left[E_0(t)\right]$ of each optimal field without noise is presented. The second and third rows of Table II show that the optimal control can fight against amplitude noise by increasing the fluence F_0, although the effect of noise is always deleterious. The variance σ_N naturally increases as the amplitude Γ_A rises. The last three rows of Table II reveal that optimal control fields can be found that are fully robust to strong phase noise with small yield variance. This result may appear to be surprising, as proper adjustment of control field phase is often viewed as necessary for attaining a good quality control yield[32]. Table III further examines this issue where it is found that robustness at any level of noise assures robustness at other levels. However, this result alone does not reveal the degree of average coherence maintained in the dynamics. The shot-to-shot signal averaged density matrix of the quantum system can be defined as:

$$\rho(t) = \frac{1}{M}\sum_{i=1}^{M}\rho^{(i)}(t) \tag{11a}$$

$$\rho^{(i)}(t) = \left|\psi\left(\left[E^{(i)}(t)\right],t\right)\right\rangle\left\langle\psi\left(\left[E^{(i)}(t)\right],t\right)\right| \tag{11b}$$

Here, $\left|\psi\left(\left[E^{(i)}(t)\right],t\right)\right\rangle$ is the state driven by the i-th field in Eq.(5) from the ensemble. The density matrix is further decomposed into its coherent and diagonal portions, $R_c(t)$, $R_d(t)$, respectively,

$$R_c(t) = \sum_{k\neq j}\left|\rho_{kj}(t)\right|^2; \qquad R_d(t) = \sum_{k}\left|\rho_{kk}(t)\right|^2 \tag{12a}$$

$$R(t) = \sum_{k,j}\left|\rho_{kj}(t)\right|^2 = R_c(t) + R_d(t) = \mathrm{Tr}\left[\rho^2(t)\right]. \tag{12b}$$

Figure 3 plots these measures of the density matrix and the state populations of the system driven by the field in the last row of Table II with strong phase noise $\Gamma_\theta = \pi$. Figure 3(a1) shows that the high level of phase noise totally destroys the coherence of the system ($R_c(t) \simeq 0$) while Figure 3(b1) shows that large coherence is built up by the same control if no noise is present. The state populations are also shown in Figures 3(a2) and 3(b2) indicating in both cases that the target goal is reached via a simple four-step ladder climbing pathway which is evidently not sensitive to phase. The result in Figure 3 needs to be understood in the context that $\rho^{(i)}(t)$, for the arbitrary $i-th$ member of the ensemble, will generally have a significant degree of coherence along its evolution. The details of the shot-to-shot coherence changes rather randomly such that $R_c(t) \simeq 0$, but the noise average $\langle\mathrm{Tr}\rho^2\rangle$ could contain a coherent contribution. Further insight into this situation will be analyzed upon examination of model 2 in Section 4.2.

If we accept a low control yield outcome, very different control behavior is found in the presence of noise. The results from optimizing Eq.(8) are shown in Table IV with various levels of amplitude and phase noise. In all cases the target yield is $O_T = 2.25\%$. Table IV shows that low field amplitude noise ($\Gamma_A \leq 0.01$) has little impact on the control outcome. Additional amplitude noise becomes more helpful indicated by the reduced control field fluence. In the domain $0.06 \leq \Gamma_A \leq 0.08$, the control outcome is much larger than the sum of the yield from the control field and noise alone. For example at $\Gamma_A = 0.07$ the noise and optimal field alone, respectively, produce yields of 0.26% and 0.16%. But, the same field operating in the presence of the noise produces a yield 2.11%. This behavior indicates that the field is cooperating with the presence of noise to more effectively achieve the posed goal. The left and right variance, σ_N^- and σ_N^+, respectively, indicate a very asymmetric distribution having a long tail on the high population side. Again, we also find several solutions that are very stable to phase noise. The collective results for amplitude noise are plotted in Figure 4.

Figure 5 shows the evolution of the density matrix measures R_c, R_d and R in Eq.(12) at different field noise amplitude Γ_A levels. With strong noise there is little surviving coherence indicated by R_c, except in the time around t$\sim$ 100 fs. In order to further explore the robust nature of the controlled dynamics in this low yield regime, Table V presents the outcome of applying noise at the amplitude Γ'_A to a field optimally determined at noise amplitude Γ_A. The yield for $E^{op}_{\Gamma_A}$ with $\Gamma'_A = \Gamma_A$ is the outcome for the field optimally determined with the noise at Γ_A. It is evident that once a field cooperates with noise at level Γ_A, then it cooperates with noise at any other level. We may conclude that at low yield, cooperation can be arranged, but at the expense of coherence.

B. Model 2

Model 2 extends the Hamiltonian of model 1 in Figure 1(a) to allow for two quanta transitions: $\omega_{02} = 2.692$, $\omega_{13} = 1.942$, $\omega_{24} = 1.314$ in rad$\cdot$fs^{-1}, with transition dipole elements: $\mu_{02} = -0.1079$, $\mu_{13} = -0.1823$, $\mu_{24} = -0.2786$, in 1.0×10^{-30} C$\cdot$m. Table VI shows that for a high target yield of $O_T = 100\%$, the control field can again effectively fight against amplitude noise by increasing the fluence F_0. But, as with the results in Table II, increasing the amplitude of the noise makes this battle harder with the final average yield decreasing and the variance increasing. The case of pure phase noise at $\Gamma_\theta = 1.0$ shows sensitivity to its presence with the yield falling to 68%. The last row of Table VI also shows a solution that is extremely robust to phase noise with reduced variance at a surprisingly small fluence(i.e., the fluence is even smaller than for the case $\Gamma_A = 0.0$.) This latter behavior is likely the result of there being many solutions to the optimal control search process with the algorithm finding alternative solutions under different circumstances.

Table VII further analyzes the robustness of the last two phase noise contaminated fields in Table VI. When the field $E^{op}_{0.0}$ (i.e., determined with no noise) is applied with a high level of phase noise, at $\Gamma_\theta = 2.0$, there is poor robustness with the final yield dropping to 24.2%. However, for the yield optimally determined at the high noise level $\Gamma'_\theta = 2.0$, there is robustness to lower levels of noise. The power spectra for the field optimized at $\Gamma_\theta = 0.0$ and 2.0 are shown in Figure 6. Comparing the two plots we see that $E^{op}_{2.0}(t)$ drives the system along a path of single quantum transitions while $E^{op}_{0.0}(t)$ drives the system as well with the additional two quanta transition $2 \rightarrow 4$. The presence of the extra two quantum transition can set up a delicate situation which is sensitive to phase noise, as Table VII indicates. The robustness of the single quantum path for $\Gamma_\theta = 2.0$ is analogous to what was found in model 1.

Two tables similar as Table IV and V but for model 2 can be constructed to show strong cooperation between optimal control field and noise when target yield is low ($O_T = 3.65\%$), and the data can be plotted to form a figure analogous to that of Figure 4.

C. Model 3

This model is same as model 1, but amplitude noise is only present in the $0 \leftrightarrow 1$ transition. Thus, noise alone cannot drive any population into the target state. There is also no phase noise in any of the transitions. Table VIII shows the results from different levels of $0 \leftrightarrow 1$ amplitude noise for a low yield target of $O_T = 10\%$. There is little evidence of cooperation with the noise, except in the last row with $\Gamma_A = 0.2$. In this case, the field fluence is low and the yield from the field alone is almost zero. But, the desired target is achieved when the field cooperates with the noise. Figure 7 shows the power spectrum of the optimal field for this case and it is evident that the $0 \leftrightarrow 1$ transition is absent. The mechanism of cooperation is clear: noise drives the system from level 0 to level 1, then the control field drives it to level 4. The remaining cases in Table VIII do not exclude the possibility that fields could be found that also cooperate with other levels of noise. The result at $\Gamma_A = 0.20$ shows that such noise cooperative solutions exist.

D. Model 4

The fourth model is the more complex two-path system in Figure 1(b). In this model, population can be transferred to the target state $|4\rangle$ along two separate pathways. The transition frequencies and dipoles of the left path are same as that of model 1; the right path has the distinct transition frequencies: $\omega_{0'1'} = 2.153$, $\omega_{1'2'} = 1.346$, $\omega_{2'3'} = 0.345$, $\omega_{3'4'} = 0.162$ in rad·fs^{-1} and dipole elements: $\mu_{0'1'} = 0.6526$, $\mu_{1'2'} = 0.7848$, $\mu_{2'3'} = 0.9023$, $\mu_{3'4'} = 1.0322$ in 1.0×10^{-30} C·m. For simplicity, along both paths only single quanta transitions are allowed.

The results in Table IX show cooperation between the field and the noise in model 4 for a low target yield of $O_T = 2.25\%$. Figure 8 shows the power spectra of the three optimal fields in Table IX. Panel (a) indicates that in the case of no noise the field primarily drives system along the right path. When noise is present in the left path (panel (b)), the optimal field drives the system along the left path in order to cooperate with the noise. Similarly, when the noise is in the right path (panel (c)), the optimal field drives the system along the right path. An interesting feature of case (c) is the lack of intensity for the last step $|3'\rangle \rightarrow |4'\rangle$ along the path. Evidently the optimal field fully draws on the noise for this step as a special case of cooperation. The presence of the fluence term in the cost function favors such behavior provided that the target goal can be met.

These results clearly show that efficiently achieving the yield is the guiding principal dictating the nature of the control field and mechanism in this case. This behavior reflects the nature of the cost function in Eq.(7), which places no demand on the coherence of the dynamics, but only asks that the control be efficiently achieved with $\alpha > 0$. If coherence maintenance was also included in the cost function the field would be guided accordingly, in keeping with the ability to meet the newly posed objective.

V. CONCLUSIONS

The impact of amplitude and phase noise upon quantum control is explored in this paper with particular emphasis on these being strong. Numerical simulations from several cases suggest that control fields can be found that either cooperate with or fight against noise, depending on the circumstances. In the case of low target yields, the control field can effectively cooperate with amplitude noise to drive the dynamics while minimizing the control fluence. In this regime pure phase noise has little impact, if the pathway to the target involved single quanta transitions. But, phase noise was found to be disruptive if there are multiple interfering pathways. Optimal solutions were also found that exhibited stability with respect to phase noise while maintaining high yields. In general, when successfully either fighting or cooperating with significant noise, the expense paid is a measured loss of dynamical coherence. In some applications a lack of full coherence can be tolerated.

The interaction between the noise and field driven dynamics is generally a highly nonlinear process. The noise can be constructive[23] or destructive[9] in the manipulation of quantum dynamics, improve[24, 25] or reduce[38] the convergence rate of searching processes, and this disparate behavior makes it difficult to precisely identify the impact of noise under various circumstances. This work explored several special cases to reveal what may happen when searching for optimal controls in the presence of field noise; a mathematical analysis of the observed behavior may also be carried out[32]. The ability to find robust, and even cooperative solutions, is most encouraging. These results are consistent with a recent analysis [7] arguing that optimally controlled quantum dynamics has a special inherent degree of robustness. Although, each case will likely have its own unique characteristic behavior, the findings are encouraging for the ability to manipulate quantum dynamics even with severe noise being present. It would also be interesting to explore these issues in the laboratory by selectively introducing measured levels of noise into the control field.

Acknowledgments

The author acknowledge support from the National Science Foundation and an ARO MURI grant. We gratefully acknowledge many valuable conservation with Mark Dykman on this work.

---

[1] S. A. Rice and M. Zhao, *Optical Control of Molecular Dynamics* (Wiley, New York, 2000).

[2] H. Rabitz, Theor. Chem. Acc. **109**, 64 (2003).

[3] I. Walmsley and H. Rabitz, Phys. Today **56**, 43 (2003).

[4] T. Brixner, N. H. Damrauer, and G. Gerber, in *Advances in Atomic, Molecular, and Optical Physics*, edited by B. Bederson and H. Walther (Academic, San Diego, CA, 2001), vol. 46, pp. 1–54.

[5] W. Zhu and H. Rabitz, J. Chem. Phys. **118**, 6751 (2003).

[6] J. M. Geremia, W. Zhu, and H. Rabitz, J. Chem. Phys. **113**, 10841 (2000).

[7] H. Rabitz, Phys. Rev. A **66**, 63405 (2002).

[8] R. Walser, H. Ritsch, P. Zoller, and J. Cooper, Phys. Rev. A **45**, 468 (1992).

[9] I. R. Sola and H. Rabitz, J. Chem. Phys. **120**, 9009 (2004).

[10] O. E. Akramine, A. Makhoute, M. Zitane, and M. Tij, Phys. Rev. A **58**, 4892 (1998).

[11] O. E. Akramine and A. Makhoute, J. Phys. B **31**, 4349 (1998).

[12] R. S. Judson and H. Rabitz, Phys. Rev. Lett **68**, 1500 (1992).

[13] L. Gammaitoni, P. Hänggi, P. Jung, and F. Marchesoni, Rev. Mod. Phys. **70**, 223 (1998).

[14] D. Zeidler, S. Frey, K.-L. Kompa, and M. Motzkus, Phys. Rev. A **64**, 23420 (2001).

[15] J. Kunde, B. Baumann, S. Arlt, F. Morier-Genoud, U. Siegner, and U. Keller, Appl. Phys. Lett. **77**, 924 (2000).

[16] T. Brixner, N. H. Damrauer, P. Niklaus, and G. Gerber, Nature (London) **414**, 57 (2001).

[17] R. J. Levis, G. M. Menkir, and H. Rabitz, Science **292**, 709 (2001).

[18] C. Daniel, J. Full, L. González, C. Lupulescu, J. Manz, A. Merli, Š. Vajda, and L. Wöste, Science **299**, 536 (2003).

[19] A. Assion, T. Baumert, M. Bergt, T. Brixner, B. Kiefer, V. Seyfried, M. Strehle, and G. Gerber, Science **282**, 919 (1998).

[20] F. Grossmann, T. Dittrich, P. Jung, and P. Hänggi, J. Stat. Phys. **70**, 229 (1993).

[21] P. Blanchard, G. Bolz, M. Cini, G. F. Deangelis, and M. Serva, J. Stat. Phys. **75**, 749 (1994).

[22] J. S. Shao, C. Zerbe, and P. Hänggi, Chem. Phys. **235**, 81 (1998).

[23] B. G. Klappauf, W. H. Oskay, D. A. Steck, and M. G. Raizen, Phys. Rev. Lett. **81**, 1203 (1998).

[24] P. Gross, D. Neuhauser, and H. Rabitz, J. Chem. Phys. **98**, 4557 (1992).

[25] G. J. Tóth, A. Lőrincz, and H. Rabitz, J. Chem. Phys. **101**, 3715 (1994).

[26] F. Shuang, C. Yang, H. Zhang, and Y. Yan, Phys. Rev. E **61**, 7192 (2000).

[27] B. E. Vugmeister and H. Rabitz, Phys. Rev. E **55**, 2522 (1997).

[28] V. N. Smelyanskiy and M. I. Dykman, Phys. Rev. E **55**, 2516 (1997).

[29] P. Pechukas and P. Hänggi, Phys. Rev. Lett. **73**, 2772 (1994).

[30] R. N. Mantegna and B. Spagnolo, Phys. Rev. Lett. **76**, 563 (1996).

[31] R. N. Mantegna and B. Spagnolo, Phys. Rev. Lett. **84**, 3025 (2000).

[32] F. Shuang, M. I. Dykman, and H. Rabitz, unpublished.

[33] D. E. Goldberg, *Genetic Algorithms in Search, Optimization, and Machine Learning* (Addison-Wesley, Reading, MA, 1989).

[34] A. N. Aizawa and B. W. Wah, in *Proceedings of the Fifth international conference on Genetic Algorithms, Urbana-Champaign, IL, USA, June 1993*, edited by S. Forrest (Morgan Kaufmann, San Mateo, CA, 1993), pp. 48–55.

[35] B. L. Miller, Ph.D. thesis, University of Illinois at Urbana-Champaign, Urbana (1997).

[36] J. Seijas, C. Morató, and J. L. Sanz-González, in *Proceedings of the Fourth International Conference on Parallel Processing and Applied Mathematics*, edited by V.R.Wyrzykowski, J. Dongarra, M.Paprzycki, and J.Wasniewski (Springer, London, UK, 2002), pp. 617–625.

[37] F. Yip, D. Mazziotti, and H. Rabitz, J. Chem. Phys. **118**, 8168 (2003).

[38] S. Rana, L. D. Whitley, and R. Cogswell, in *Proceedings of the Fourth International Conference on Parallel Problem Solving from Nature*, edited by H. Voigt, W. Ebeling, I. Rechenberg, and H.-P. Schwefel (Springer, Berlin, 1996), pp. 198–207.

Table I. Population distribution of the single path model 1 when the system is only driven by amplitude noise.

	Population in the state				
Γ_A [a]	0	1	2	3	4
.10	41.6%	32.1%	17.9%	6.1%	2.25%
.09	44.0%	34.4%	16.0%	4.4%	1.24%
.08	47.8%	35.9%	12.9%	2.8%	0.63%
.07	54.1%	34.1%	9.8%	1.7%	0.26%
.05	69.8%	26.0%	3.9%	0.35%	0.026%
.03	86.8%	12.5%	0.68%	0.023%	0.0006%
.01	98.4%	1.6%	0.0096%	3.6×10^{-5}%	1.0×10^{-7}%
.00	100%	0%	0%	0%	0%

[a] The nominal field is zero: $A_l^0 = 0$, and there is no phase noise: $\gamma_{\theta_l}^{(i)} = 0.0$; Γ_A is the maximum noise amplitude: $\left|\gamma_{A_l}^{(i)}\right| \leq \Gamma_A$, in Eq.(4).

Table II. Optimal control field fighting against amplitude and phase noise with model 1 for the high target yield $O_T = 100\%$

Γ_A,Γ_θ [a]	$\left\langle O\left[E_n^{(i)}(t)\right]\right\rangle_N$ [b]	F_0 [c]	$O\left[E_0(t)\right]$ [d]	F_n [e]	$\left\langle O\left[E^{(i)}(t)\right]\right\rangle_N$ [f]	σ_N
0,0	0.00%	0.066	98.7%	0.00	98.7%	0%
0.05,0	0.026%	1.73	98.6%	3.3×10^{-3}	89.4%	5.31%
0.10,0	2.25%	12.3	95.8%	1.3×10^{-2}	73.6%	13.1%
0,1	-	0.065	97.8%	-	97.1%	0.65%
0,2	-	0.065	95.9%	-	96.2%	1.04%
0,π	-	0.065	97.7%	-	96.0%	1.08%

[a] Γ_A, Γ_θ are the maximum of the amplitude and phase noise, respectively: $\left|\gamma_{A_l}^{(i)}\right| \leq \Gamma_A$, $\left|\gamma_{\theta_l}^{(i)}\right| \leq \Gamma_\theta$.

[b] $\left\langle O\left[E_n^{(i)}(t)\right]\right\rangle_N$: Yield from noise alone (Eq. (10)) without a control field.

[c] Fluence of the control field (Eq.(3b)).

[d] $O\left[E_0(t)\right]$: Yield arising from the control field (Eq.(2a)) without noise.

[e] Fluence of the noise.

[f] $\left\langle O\left[E^{(i)}(t)\right]\right\rangle_N$: Yield from the optimal control field in the presence of noise(Eq.(6))

Table III. Yield from optimal control fields in the case of model 1 with different levels of phase noise for the high target yield of $O_T = 100\%$.

	$\left\langle O\left[E^{op}_{\Gamma_\theta}(t)\right]\right\rangle_{\Gamma'_\theta}$ [a]			
Γ'_θ	$E^{op}_{0.0}$	$E^{op}_{1.0}$	$E^{op}_{2.0}$	E^{op}_{π}
0.0	98.7%	97.8%	95.9%	97.7%
1.0	97.2%	97.1%	96.4%	96.7%
2.0	95.4%	96.1%	96.2%	96.1%
π	95.1%	95.9%	96.1%	96.0%

[a] Yield at the field $E^{op}_{\Gamma_\theta}(t)$ with phase noise: $\left|\gamma^{(i)}_{\theta_l}\right| \leq \Gamma'_\theta$. Here $E^{op}_{\Gamma_\theta}(t)$ is the field for which the yield was optimized (i.e., the diagonal elements in the Table) at the phase noise level Γ_θ.

Table IV. Optimal control with both amplitude and phase noise for model 1 with a low objective yield of $O_T = 2.25\%$.

Γ_A,Γ_θ [a]	$\left\langle O\left[E_n^{(i)}(t)\right]\right\rangle_N^b$	F_0 [c]	$O\left[E_0(t)\right]^d$	F_n [e]	$\left\langle O\left[E^{(i)}(t)\right]\right\rangle_N^f$	$\sigma_N(\sigma_N^-, \sigma_N^+)$ [g]
0.10,0	2.25%	0.00	0.00%	1.33×10^{-2}	2.25%	4.7%(2.0%,10%)
0.09,0	1.24%	3.1×10^{-3}	2×10^{-6}	1.02×10^{-2}	2.09%	5.8%(1.8%,12%)
0.08,0	0.63%	6.1×10^{-3}	2.5×10^{-5}	8.53×10^{-3}	2.17%	6.5%(2.0%,15%)
0.07,0	0.26%	8.4×10^{-3}	0.16%	6.53×10^{-3}	2.11%	5.9%(2.0%,13%)
0.05,0	0.026%	9.9×10^{-3}	1.34%	3.33×10^{-3}	2.08%	4.7%(1.8%,9.3%)
0.03,0	6.0×10^{-4}%	1.06×10^{-2}	1.87%	1.20×10^{-3}	2.06%	2.6%(1.4%,4.1%)
0.01,0	1.0×10^{-7}%	1.11×10^{-2}	2.12%	1.33×10^{-4}	2.17%	0.8%(0.7%,1.0%)
0,0.5	-	1.09×10^{-2}	2.18%	-	2.17%	0.01%
0,1.0	-	1.10×10^{-2}	2.21%	-	2.18%	0.03%
0,2.0	-	1.10×10^{-2}	2.19%	-	2.17%	0.03%
0,0	-	1.09×10^{-2}	2.20%	-	2.20%	0.00%

[a,b,c,d,e,f] refer to Table II.

[g] σ_N^-, σ_N^+ are left and right standard deviation, respectively, around the mean in [f].

Table V. Yield from optimal control fields with different levels of amplitude noise for model 1.

	$\left\langle O\left[E^{op}_{\Gamma_A}(t)\right]\right\rangle_{\Gamma'_A}$ [a]							
Γ'_A	$E^{op}_{0.10}$	$E^{op}_{0.09}$	$E^{op}_{0.08}$	$E^{op}_{0.07}$	$E^{op}_{0.05}$	$E^{op}_{0.03}$	$E^{op}_{0.01}$	$E^{op}_{0.00}$
0.10	2.25	2.98	4.15	4.35	4.64	4.74	5.25	5.50
0.09	1.24	2.09	2.96	3.80	3.99	4.11	4.79	4.53
0.08	0.63	1.27	2.17	2.92	3.28	3.60	4.16	3.76
0.07	0.26	0.71	1.48	2.11	2.90	3.18	3.48	3.46
0.05	0.026	0.17	0.55	1.1	2.08	2.50	2.91	3.36
0.03	6.0×10^{-4}	0.023	0.14	0.44	1.58	2.06	2.38	2.45
0.01	1.0×10^{-7}	0.0014	0.016	0.19	1.38	1.88	2.17	2.21
0.00	0.00	0.00020	0.0025	0.16	1.34	1.87	2.12	2.20

[a] Yield at $E^{op}_{\Gamma'_A}(t)$ with noise bounded by $|\gamma_{A_l}| \leq \Gamma'_A$ and for $\gamma_\theta = 0$. Here $E^{op}_{\Gamma_A}(t)$ is field for which the yield (i.e., the diagonal elements in the table) was optimized with noise $\Gamma'_A = \Gamma_A$. The yields are expressed in percent.

Table VI. The yield from optimal control fields fighting with amplitude or phase noise in model 2 with the high yield target objective of $O_T = 100\%$.

Γ_A,Γ_θ [a]	$\left\langle O\left[E_n^{(i)}(t)\right]\right\rangle_N$ [b]	F_0 [c]	$O\left[E_0(t)\right]$ [d]	F_n [e]	$\left\langle O\left[E^{(i)}(t)\right]\right\rangle_N$ [f]	σ_N
0.0,0.0	0.00%	0.28	99.1%	0.00	99.1%	0.00%
0.05,0.0	0.13%	1.53	98.2%	5.83×10^{-3}	87.2%	7.4%
0.1,0.0	3.65%	3.27	93.7%	2.33×10^{-2}	66.5%	14.5%
0.0,1.0	-	0.33	80.4%	-	68.0%	13.1%
0.0,2.0	-	0.065	96.5%	-	91.6%	4.2%

[a,b,c,d,e,f] refer to Table II

Table VII. Control yields with optimal fields at different phase noise levels for the high yield target $O_T = 100\%$ in case of model 2

	$\left\langle O\left[E^{op}_{\Gamma_\theta}(t)\right]\right\rangle_{\Gamma'_\theta}$ [a]		
Γ'_θ	$E^{op}_{0.0}$	$E^{op}_{1.0}$	$E^{op}_{2.0}$
0.0	99.1%	80.4%	96.5%
1.0	42.9%	68.0%	95.3%
2.0	24.2%	37.5%	91.6%

[a] refer to Table III

Table VIII. Control outcomes from optimal fields for model 3 with a low target yield of $O_T = 10\%$.

Γ_A [a]	$\left\langle P_1\left[E_n^{(i)}(t)\right]\right\rangle_N$ [b]	F_0 [c]	$O\left[E_0(t)\right]$ [d]	$\left\langle O\left[E^{(i)}(t)\right]\right\rangle_N$ [f]	σ_N
0.00	0.00%	0.0176	9.95%	9.95%	0.00%
0.01	1.67%	0.0198	9.91%	9.94%	1.39%
0.05	31.7%	0.0229	10.66%	9.97%	3.24%
0.10	61.1%	0.0194	9.27%	9.99%	8.09%
0.20	46.6%	0.0144	0.0013%	9.90%	6.06%

[a] Amplitude noise is only in the transitions 0 ↔ 1.

[b] Population in level 1 when the system is only driven by noise.

[c,d,f] refer to Table II.

Table IX. Yield attained from the optimal fields for model 4 with the low yield target of $O_T = 2.25\%$.

$\Gamma_A^{(L)}, \Gamma_A^{(R)}$ [a]	$\left\langle O\left[E_n^{(i)}(t)\right]\right\rangle_N$ [b]	F_0 [c]	$O\left[E_0(t)\right]$[d]	$\left\langle O\left[E^{(i)}(t)\right]\right\rangle_N$ [f]
0.00,0,00	0.00%	0.0093	2.19%	2.19%
0.08,0.00	0.63%	0.0064	0.0003%	2.17%
0.00,0.07	0.50%	0.0052	0.0002%	2.08%

[a] $\Gamma_A^{(L)}, \Gamma_A^{(R)}$: Noise in the left and right paths, respectively;

[b,c,d,f] refer to Table II.

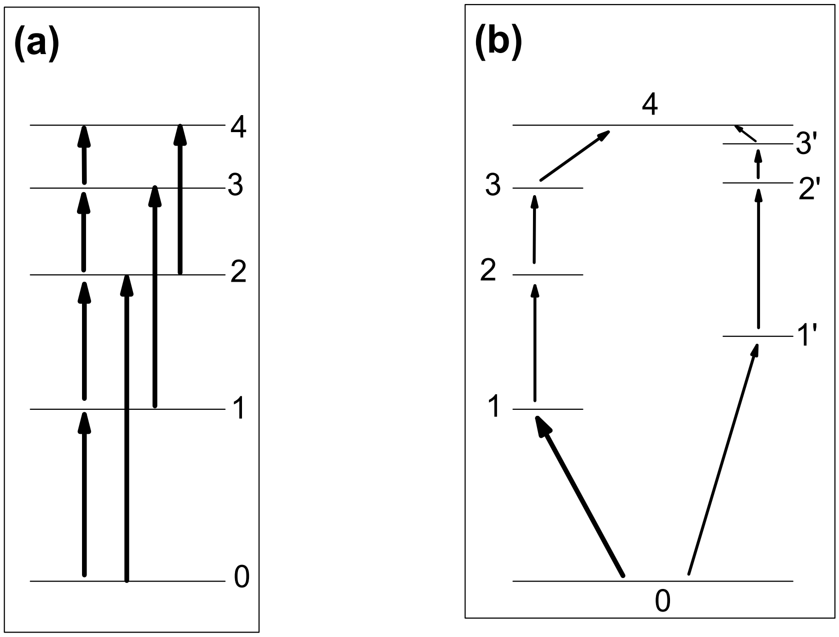

FIG. 1: Two quantum multilevel systems used to investigate the impact of noise on optimally controlled dynamics. (a) The 5 level single path system used for simulations with models 1,2,3 in Sections 4.1, 4.2, and 4.3, respectively. Model 1 and 3 only allow single quanta transitions while model 2 allows both single and double quanta transitions. (b) The double-path system for model 4 in Section 4.4.

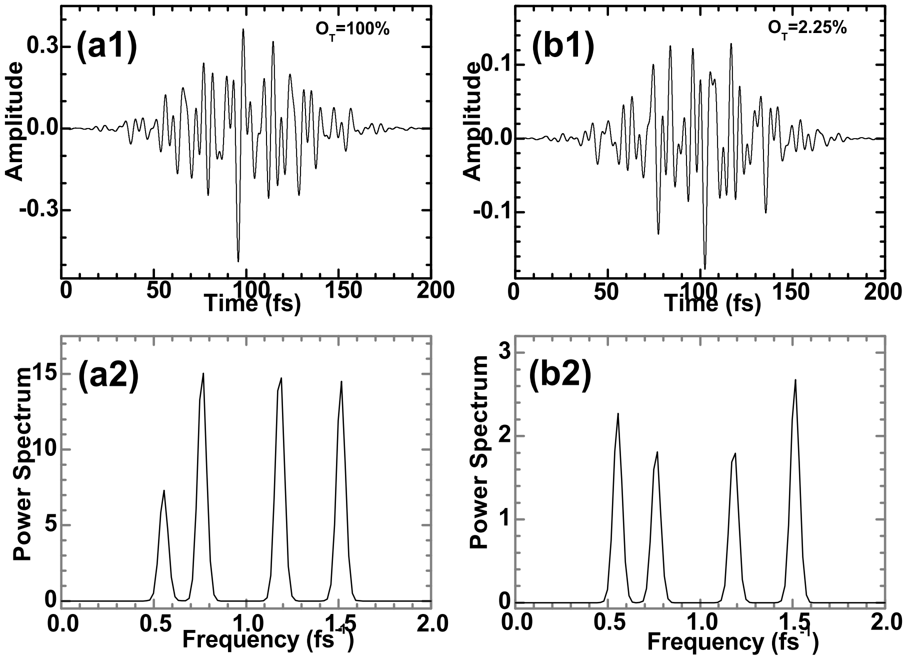

FIG. 2: Optimal control fields and their power spectra for model 1 when the field has no noise. The fields are found using the cost function in Eq.(3a). Plots (a1) and (a2) correspond to the high target yield of $O_T = 100\%$ while plots (b1) and (b2) correspond to the low target yield of $O_T = 2.25\%$.

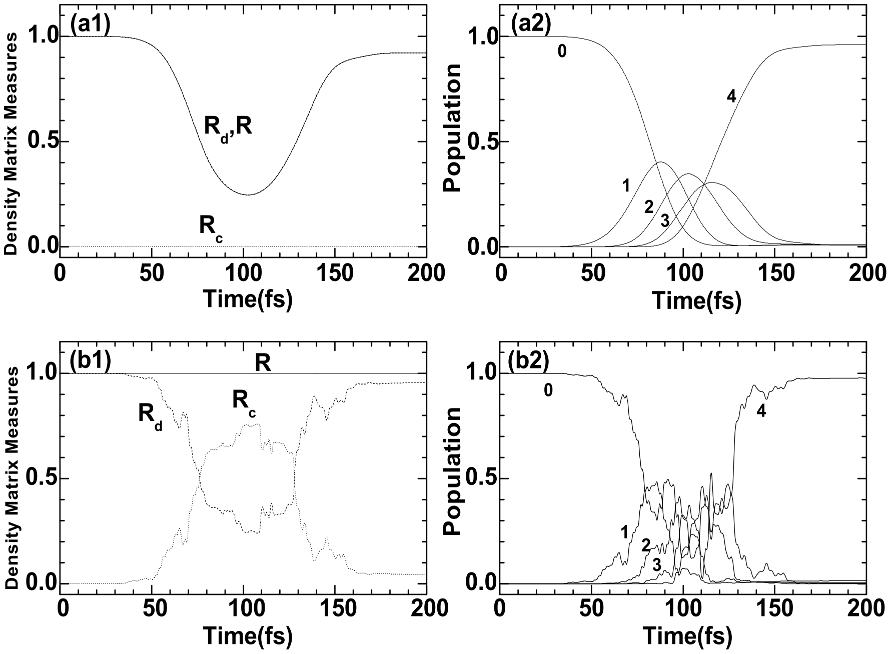

FIG. 3: The time dependence of model 1 dynamics driven by the optimal control field in the last row of Table II. The density matrix measures $R_d(t)$, $R_c(t)$, $R(t)$ in plots (a1) and (b1) are defined in Eq.(12). Plots (a1) and (a2) show the dynamics when the system is driven by a control field with noise while plots (b1) and (b2) show the dynamics of the system driven by the same field but without noise. The associated state populations are shown in plots (a2) and (b2).

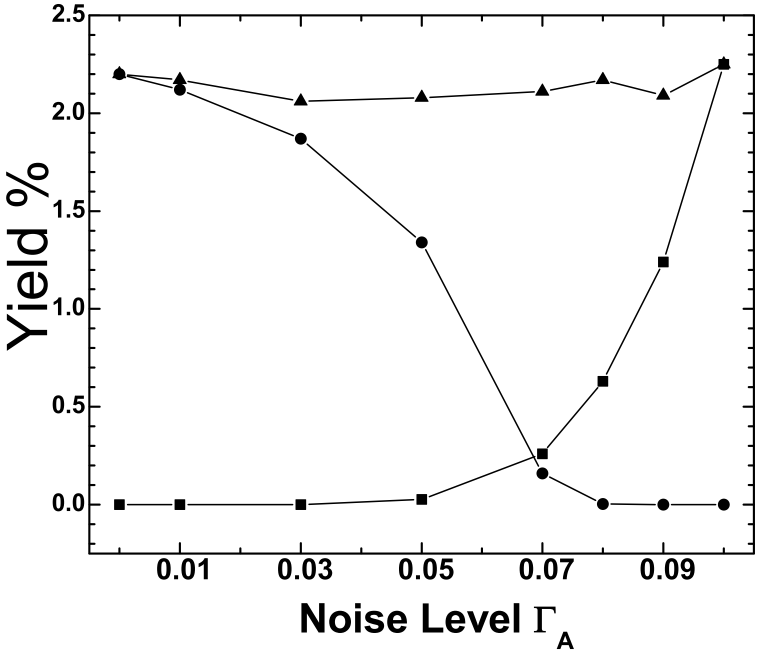

FIG. 4: The control yield under various noise conditions for model 1 with the low yield target of $O_T = 2.25\%$ in Table V. The labeled curves show the yield for noise alone, the yield for the optimal field alone and the yield for the field in the presence of noise. There is notable cooperation between the noise and the field especially over the amplitude noise range $0.06 \leq \Gamma_A \leq 0.08$.

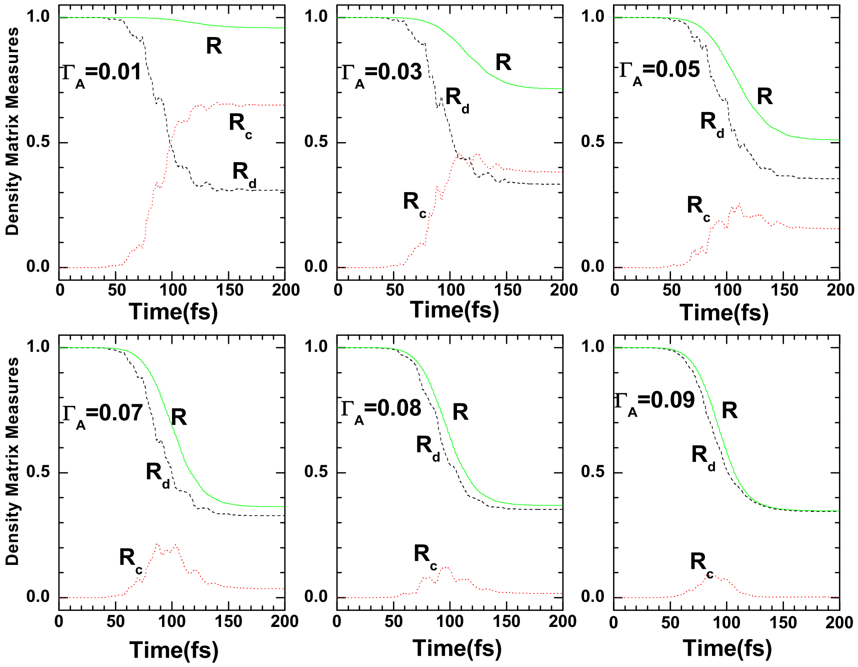

FIG. 5: Evolution of the density matrix measures in Eq.(12) with different levels of field amplitude noise for the low target yield case of Figure 4. The coherence is successively destroyed by stronger noise, but it still survives around t∼ 100 fs.

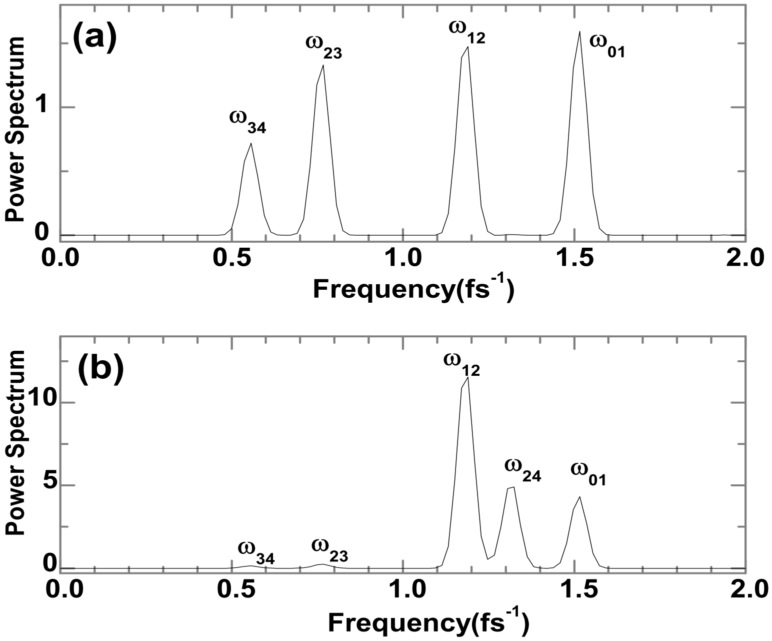

FIG. 6: Power spectra of the control fields for model 2 aiming at a high yield with $O_T = 100\%$. Plot(a) is for the field $E_{2.0}^{op}$ robust to phase noise; plot(b) is for the field $E_{0.0}^{op}$ which is not robust to noise. The robust control field in (a) avoids the extra interference arising from the two quanta transition $2 \leftrightarrow 4$.

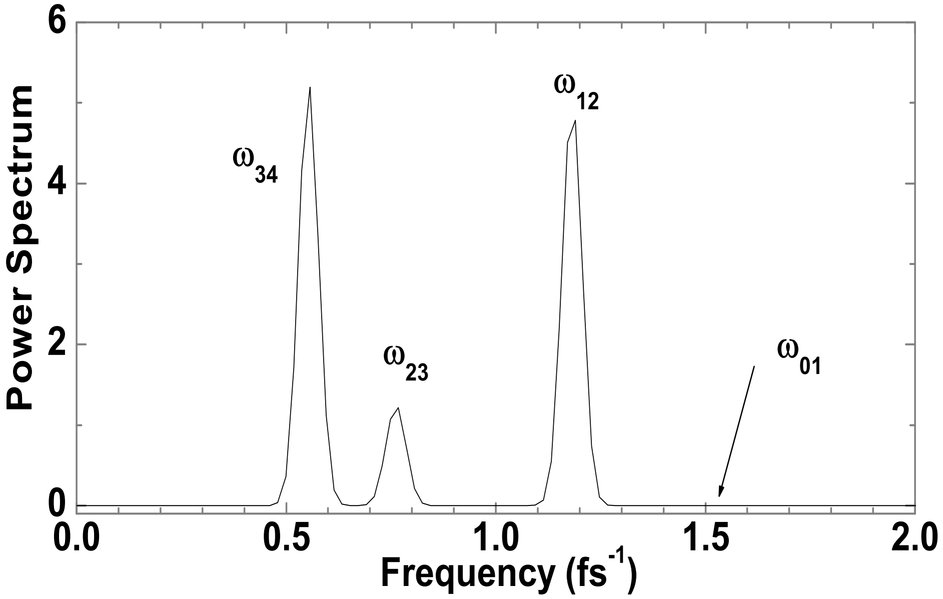

FIG. 7: The optimal field power spectra of model 3. Here noise is only in the amplitude of the $0 \leftrightarrow 1$ transition with $\Gamma_A = 0.20$. The optimal field cooperates with the noise by eliminating the ω_{01} frequency and exclusively relying on the noise to drive that step. The arrow indicates where that frequency lies.

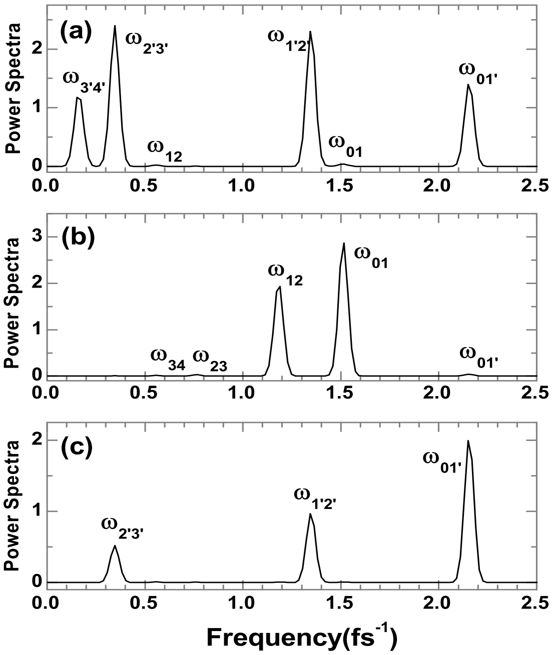

FIG. 8: Power spectra of the control fields for model 4 (see panel (b) of Figure 1). The frequencies along the right path in Figure 1 are denoted with a prime to distinguish them from the left path. (a) No noise, (b) noise in the left path, (c) noise in the right path. In these low target yield cases the optimal field cooperates with the noise and follows the associated path.